World Academy of Science, Engineering and Technology
International Journal of Geological and Environmental Engineering
Vol:18, No:4, 2024

Synthesis of Temperature Sensitive Nano/Microgels by Soap-Free Emulsion Polymerization and Their Application in Hydrate Sediments Drilling Operations

Xuan Li, Weian Huang, Jinsheng Sun, Fuhao Zhao, Zhiyuan Wang, Jintang Wang

***Abstract*—**Natural gas hydrates (NGHs) as promising alternative energy sources have gained increasing attention. Hydrate-bearing formation in marine areas is highly unconsolidated formation and is fragile, which is composed of weakly cemented sand-clay and silty sediments. During the drilling process, the invasion of drilling fluid can easily lead to excessive water content in the formation. It will change the soil liquid plastic limit index, which significantly affects the formation quality, leading to wellbore instability due to the metastable character of hydrate-bearing sediments. Therefore, controlling the filtrate loss into the formation in the drilling process has to be highly regarded for protecting the stability of the wellbore. In this study, the temperature-sensitive nanogel of P(NIPAM-co-AMPS-co-tBA) was prepared by soap-free emulsion polymerization, and the temperature-sensitive behavior was employed to achieve self-adaptive plugging in hydrate sediments. First, the effects of additional amounts of 2-acrylamido-2-methyl-1-propanesulfonic acid (AMPS), tert-butyl acrylate (tBA), and methylene-bis-acrylamide (MBA) on the microgel synthesis process and temperature-sensitive behaviors were investigated. Results showed that, as a reactive emulsifier, AMPS can not only participate in the polymerization reaction but also act as an emulsifier to stabilize micelles and enhance the stability of nanoparticles. The volume phase transition temperature (VPTT) of nanogels gradually decreased with the increase of the contents of hydrophobic monomer tBA. An increase in the content of the cross-linking agent MBA can lead to a rise in the coagulum content and instability of the emulsion. The plugging performance of nanogel was evaluated in a core sample with a pore size distribution range of 100-1000 nm. The temperature-sensitive nanogel can effectively improve the microfiltration performance of drilling fluid. Since a combination of a series of nanogels could have a wide particle size distribution at any temperature, around 200 nm to 800 nm, the self-adaptive plugging capacity of nanogels for the hydrate sediments was revealed. Thermosensitive nanogel is a potential intelligent plugging material for drilling operations in NGH-bearing sediments.

***Keywords*—**Temperature-sensitive nanogel, NIPAM, self-adaptive plugging performance, drilling operations, hydrate-bearing sediments.

I. Introduction

NGHs are solid ice-like structures composed of water molecules surrounding natural gas molecules (mainly methane) [1], [2]. NGHs are abundant and distribute widely in deep-water sedimentary structures and polar regions where the surroundings satisfy the specific formation conditions of low temperature and high pressure [3], [4]. However, extracting methane from gas hydrate reservoirs is challenging due to complex thermodynamic conditions and potential environmental risks associated with hydrate decomposition [5]-[8]. During the drilling process, the invasion of drilling fluid can easily invade into the reservoirs [7], [8]. When the water content increases to higher than the liquid limit, the soil changes from a plastic state to a fluid state, and there is almost no binding force between soil particles. Therefore, excessive water content in the formation can significantly reduce the formation strength, leading to wellbore instability [9]. Therefore, controlling the filtrate loss into the formation in the drilling process has to be highly regarded for protecting the stability of the wellbore [3].

During the drilling operations in the conventional oil/gas reservoirs, the positive differential pressure impels nanoparticles to enter the reservoirs, randomly embedded in the pore space. The nanogels can form gradually a dense filter cake on the surface of the reservoir, effectively controlling the filtration and preventing the drilling fluid from intruding into the pore space in the sediment. Therefore, various nanoparticles were prepared and used in the drilling fluids [10]-[13]. For instance, Zhong et al. synthesized β-cyclodextrin polymer microspheres (β-CDPMs) through the inverse emulsion polymerization method and applied them to drilling engineering under high temperature environments, achieving effective filtration control for drilling fluids [10]. Lei et al. synthesized self-crosslinking soap-free latexes using N-(hydroxymethyl)acrylamide (NAM) as a high-temperature self-crosslinker. The microporous plugging mechanism is revealed to involve heat deforming and self-crosslinking film formation, in addition to physical bridging and filling [11]. However, the pore size of reservoirs varied with the well depth, and thus nanoparticles with uniform diameters might be insufficient to plug all the pore space of formation encountered during the

Xuan Li is with the School of Petroleum Engineering, China University of Petroleum (East China), Qingdao, Shandong, 266580, P. R. China (e-mail: lixuan94sy@163.com).

Weian Huang is with the School of Petroleum Engineering, China University of Petroleum (East China), Qingdao, Shandong, 266580, P. R. China (corresponding author, phone: +86 13793290370; Fax: 0532-86982923; e-mail: masterhuang1997@163.com).

Jinsheng Sun Fuhao Zhao, Zhiyuan Wang, Jintang Wang were with China University of Petroleum (East China), Shandong, 266580, P. R. China (e-mail: sunjinsheng@petrochina.com.cn, zhaofuhao321@163.com, wangzy1209@126.com, wangjintang@upc.edu.cn).

whole drilling process.

In recent years, the development of temperature-sensitive polymers/gels has emerged as a promising approach to address this issue. Temperature-sensitive microgels can provide the varied particle sizes in different temperatures that can plug the pore space in hydrate reservoirs and prevent drilling fluid from intruding into sediments through the swelling/deswelling equilibrium. However, an important issue is to find the thermo-sensitive microgels suitable for temperature ranges in the target formation. Hydrate sediments vertically locate in the depth with the range of 200~300 mbsf below the seafloor, and the water depth is generally over 1000 m [14]. The initial temperature of hydrate reservoirs ranged generally 14~18 °C [14]-[16]. One of the widely studied thermo-responsive materials for biomedical applications is poly(N-isopropylacrylamide) (PNIPAM) which exhibits a critical transition temperature, at about 32 °C. PNIPAM micro/nanogels have been obtained by dispersion polymerization [17]-[21]. In this method the oligomers are insoluble in water at the reaction temperature (> 60 °C), and act as the reaction nuclei for the formation of the nanogels [20], [21]. Even though the VPTT of PNIPAM-based microgel is close to the temperature of hydrate sediment, tuning the transition temperature is crucial for tailoring their properties for specific applications for drilling fluids in hydrate formations. The has been modified by copolymerization with different organic comonomers. Kubo et al. developed the poly(NIPAM-co-HEMA) using an ultrasonic polymerization technique to tune the LCST from 32.5 °C to 12.1 °C [22]. Wang et al. increased the LCST of thermos-responsive copolymer by introduction of ethylene glycol methacrylate (EGMA) monomers into n-isopropylacrylamide (NIPAM) [23]. Huang et al. prepared a thermo-responsive random copolymer of poly (NIPAm-co-FMA) within a lower LCST (15-28 °C) [24]. Serrano-Medina et al. successfully prepared core-shell structured nano/microgels with a crosslinked N-isopropylacrylamide (NIPAAm) core and a poly(ethylene glycol) methyl ether methacrylate (PEGMA) and 2-methacryloyloxybenzoic acid (2MBA) shell.

In this study, we aimed to synthesize temperature-sensitive nanogel of P(NIPAM-co-AMPS-co-tBA) using the soap-free emulsion polymerization, tuning its VPTT to achieve a closer temperature with gas hydrate reservoirs. The temperature-responsive behavior of the microgels were characterized by dynamic light scattering (DLS) method. First, the influence of the amounts of AMPS, tBA and cross-linker MBA on the process of copolymerization were studied, followed by the changes of microgels VPTT. The self-adaptive plugging performance was studied in a core sample with heterogeneity. Stimuli-responsive materials to environmental conditions will have the potential to become innovative competitors in the NGH drilling and development operations in the future.

II. Materials and Methods

A. Materials

N-isopropyl acrylamide, tert-Butyl acrylate (tBA), and 2-Acrylamido-2-methylpropane sulfonic acid (AMPS) were all purchased from Aladdin Biochemical Technology Co., Ltd. (Shanghai, China). Ammonium persulphate (APS), potassium chloride (KCl) and N,N'-methylene Bis-acrylamide (MBA) were obtained from Sinopharm Chemical Reagent Co., Ltd. (Shanghai, China). All chemicals were of analytical grade and were used without further treatment. Core sample was obtained from Southwest Oilfield Company. Deionized water was utilized in this work.

B. Synthesis of Temperature-Responsive Polymers

Thermosensitive microgels of P(NIPAM-co-AMPS-tBA) were prepared by soap-free emulsion polymerization. The designed amount of NIPAM, AMPS, tBA monomer and cross-linking agent MBA were added into 45 mL of deionized water, and intensively stirred for 30 min after pouring them into a 250 mL four-necked flask (equipped with a thermometer, an electric stirrer, a condenser tube and a nitrogen gas inlet). AMPS was applied as a reactive emulsifier. It was expected that the hydrophilic AMPS segments were distributed on the surface of latex particles through the semi-continuous process to stabilize the soap-free latex particles. The mixture was stirred at 300 rpm under N2 atmosphere for 20 min. After that, heating the mixture up to 70 °C, initiator APS aqueous solution (5 mL) was added. The solution gradually changed from transparent to light blue, and then the nanogel was obtained appearing opalescence after 6 h reaction. The latexes were then cooled to room temperature, followed by filtering through a 200-mesh screen to remove generated coagulum. A cellulose dialysis membrane to dialyze the obtained polymer microgel emulsion in water for 7 days to remove unreacted monomers and cross-links. The treated microgel emulsion was rapidly frozen in liquid nitrogen, then dried in a freeze dryer for 24 hours to obtain a powdery solid.

C. Nano/Microparticle Characterization

The thermo-responsive behaviors of nanogels were revealed by particle size distribution and morphological observation. Herein, the hydrodynamic diameters (Dh) of microgels were measured by DLS on a nanoparticle size analyzer (Brookhaven, USA) equipped with a temperature control table. A small amount of purified microgel emulsion was taken and diluted 50 times with ultrapure water. A sufficient dispersion of the suspension in water by ultrasonic vibration was followed by the hydrodynamic diameter measurements of the microgel at different temperatures (25 °C~55 °C/2 °C). The samples were equilibrated for at least 10 min at each temperature before DLS measurements to ensure that the microgels reached the swelling/deswelling equilibrium in aqueous medium. The DLS tests were conducted three times at each temperature (interval 2 min), and the average values were obtained as the hydrodynamic diameter of the microgel [25].

The morphological characteristics of microgel latexes were observed through SEM and TEM images, which were carried out on an S-4800 field emission scanning electron microscope (Hitachi, Japan) with an accelerating voltage of 20 kV and a JEM 2100F transmission electron microscopy (JEOL, Japan) with an accelerating voltage of 200 kV, respectively. The freeze-dried powdered microgel was fully dispersed in absolute

ethanol by ultrasonic vibration. Then the dispersion was dropped on the copper grid with a micro-syringe, and dried it at room temperature for 24 hours. After that, the morphology and particle size of microgels were observed using SEM/TEM.

D.Evaluation method of Plugging Performance of Microgels

In order to evaluate the plugging performance of thermosensitive microgels in sediments, an experimental apparatus in this study was assembled and modified based on the previous work reported by Ji et al. [26]. The schematic diagram of the setup is shown in Fig. 1. Two independent piston containers were employed to inject KCl brine and microgel suspensions, respectively. In the process of plugging performance evaluation, all data from various transducers were collected and transferred in a specialized software. This established experimental setup possesses the controllable and adjustable temperature to investigate plugging performance at a specific temperature.

The 3 wt% KCl brine is used to eliminate the influence of clay swelling. A series of microgel suspensions with different content of tBA (TMG-B05, TMG-B10, TMG-B25, TMG-B40, TMG-B55) were prepared and added into water to obtain a mixture with a wide range of particle size. To evaluate the plugging performance of the temperature-sensitive microgels in heterogeneous sediments, a core sample with a wide particle size distribution was adopted [27], [28].

The core sample saturated with KCl brine was crammed into the core holder, and confining pressure of 2 MPa was exerted in the core. Then, KCl brine was forward injected into the cores using the injection pump with a flow rate of 1.0 mL/min until the displacement differential pressure (ΔP) was stable. After that, the microgel suspension was injected into the plugged core and the pressures were recorded over time at the temperature of 25 ℃. When the plugging test completed, the KCl brine was injected into the core again to compare the ΔP values with that before microgel suspension injection. Note that the confining pressure should be always keep 1.5~2.0 MPa higher than the inlet pressure.

After the plugging evaluation, in order to verify the microscopic mechanism of plugging in core structures, the microscopic morphology of core sample before and after core flow tests were investigated.

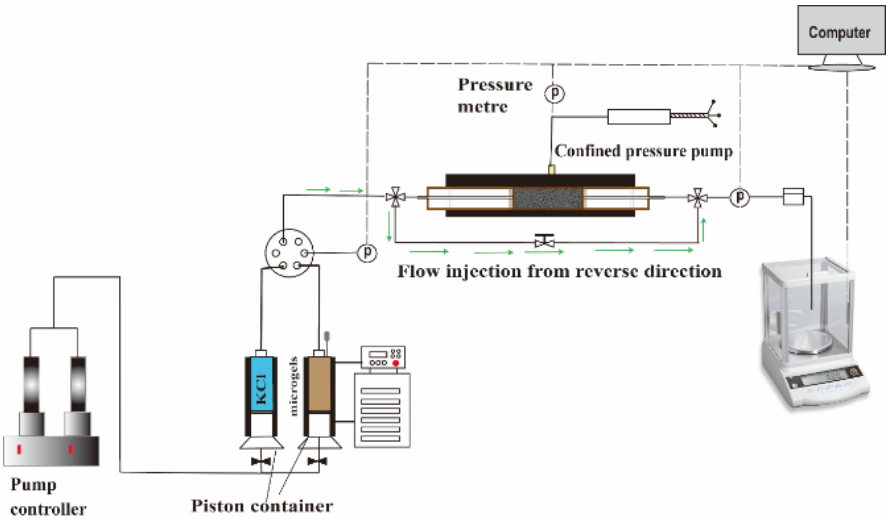

Fig. 1 A schematic diagram of the experimental apparatus

III. Results and Discussion

A series of P(NIPAM-co-AMPS-co-tBA) microgels with different ratios of monomers were prepared by soap-free emulsion polymerization in the presence of MBA as crosslinker and APS as initiator. Fig. 2 demonstrates the scheme for the synthesis of P(NIPAM-co-AMPS-tBA) microgel. Due to the strong hydrophobicity of the monomer tBA, it is difficult to disperse directly in water without emulsifiers and copolymerize with main chains. Although NIPAM has solubilization effect due to the coexistence of hydrophilic group and hydrophobic group isopropyl group in the molecular structure, it should be noted that the micelles are easy to aggregate to form a large coagulum. The unsaturated double bonds (C=C) of AMPS allow it participated in free radical copolymerization. Meanwhile, its amide groups and sulfonic acid groups give it the properties of an emulsifier. Therefore, the presence of AMPS can stabilize the micelles, thereby preparing uniform and stable microgel particles.

A. Effect of AMPS Content

Table I shows the physicochemical characteristics and monomer conversion of the microgels with different contents of AMPS.

Results showed that, in the absence of AMPS, the coagulum content of the reaction mixture reached 87.27%, which means that the majority of the monomers were not converted into nano-sized gels, but aggregated to form clotty coagulum. However, with the introduction of AMPS, the coagulum content dropped sharply. When AMPS was added at only 0.5% mol (relative to NIPAM), the coagulum content descended to 25.14%, and 78.37% of the monomers formed nanogel

particles. As the amounts of AMPS reached 1.0%, the coagulum dropped to only 1.72%, and the monomer conversion rate increased to 98.62%, indicating that most of the monomers were polymerized into microgels. When the content of AMPS increased by more than 1% (wt%), the monomer conversion and coagulum content remained a relatively constant value.

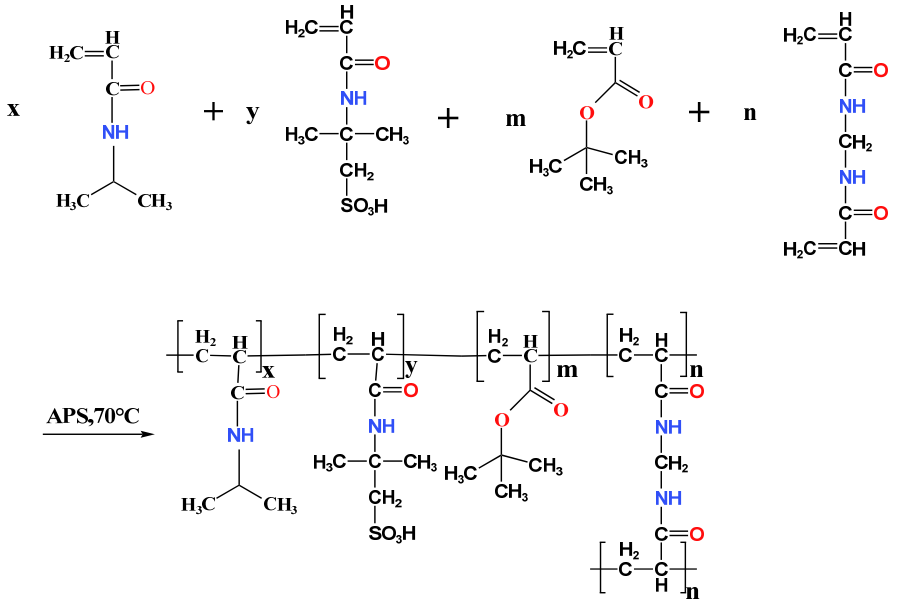

Fig. 2 Scheme for the synthesis of P (NIPAM-co-AMPS-tBA)

TABLE I
PHYSICOCHEMICAL CHARACTERISTICS OF MICROGELS WITH DIFFERENT CONTENTS OF AMPS

Sample	NIPAM (mmol)	tBA (mmol)	AMPS (mmol)	MBA (mmol)	Solid content (wt%)	Monomer conversion (%)	Coagulum content (wt%)
TMG-A00	30	1.0	0	0.3	-	-	87.27
TMG-A05	30	1.0	0.5	0.3	5.44	78.37	25.14
TMG-A10	30	1.0	1.0	0.3	6.99	98.62	1.72
TMG-A15	30	1.0	1.5	0.3	6.39	89.38	1.18
TMG-A20	30	1.0	2.0	0.3	6.68	92.72	1.14

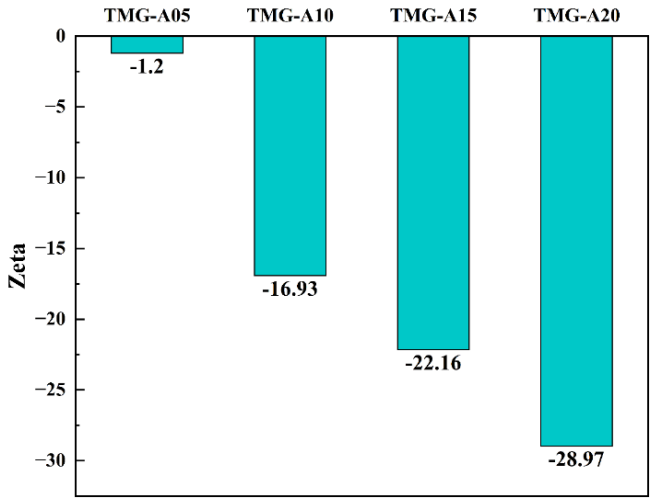

Fig. 3 Zeta potentials of microgel suspensions with different AMPS contents

AMPS can reduce the surface tension of water to some extent (52.9 mN/m at 0.02 g/mL concentration), thus facilitating the migration of AMPS molecules to the interface between monomer and water. Subsequently, as the reaction proceeds, negatively charged sulfonic acid groups were bonded on the particle surface to improve the dispersion stability, which can be verified by the results of zeta potentials (Fig. 3).

B. Effect of Crosslinker MBA

We also evaluated the effect of crosslinker concentration on nano/microgel synthesis process, as shown in Table II. The results demonstrated that with the increase of cross-linking agent content, the coagulum content and monomer conversion rate first increased and then decreased. At 1.5 mol% cross-linker (relative to NIPAAm) content, the coagulum content increased significantly, indicating the formation of precipitates or large gels during the synthesis. This is because an increase in the crosslinker content causes more nanoparticles to aggregate together, forming larger aggregations.

C. Effect of AMPS on Temperature-Responsive Behavior

Fig. 4 shows the changes of particle size distributions of microgels with different contents of AMPS at with varied temperatures. It can be seen that when the temperature increases from 25 °C to 55 °C, the hydrodynamic diameter distribution shifts to the left, meaning that the hydrodynamic diameter of

the microgels in water decreases with the increase of water temperature.

TABLE II
PHYSICOCHEMICAL CHARACTERISTICS OF MICROGELS WITH DIFFERENT CONTENTS OF MBA

Sample	NIPAM (mmol)	tBA (mmol)	AMPS (mmol)	MBA (mmol)	Solid content (wt%)	Monomer conversion (%)	Coagulum content (wt%)
TMG-M03	30	1.0	1.0	0.3	6.89	98.14	1.02
TMG-M045	30	1.0	1.0	0.45	6.84	98.37	1.27
TMG-M075	30	1.0	1.0	0.75	6.29	96.62	2.35
TMG-M15	30	1.0	1.0	1.5	5.83	86.38	15.7
TMG-M30	30	1.0	1.0	3.0	5.18	72.72	26.4

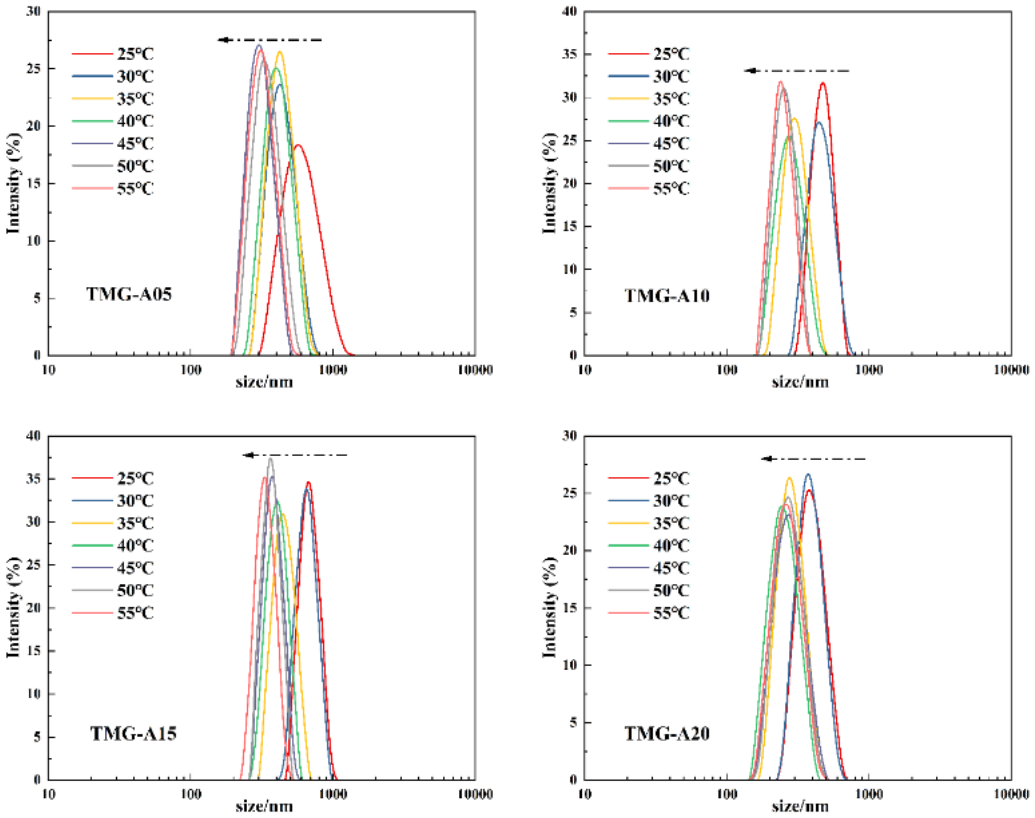

Fig. 4 Changes in particle size distribution of microgels with different AMPS content

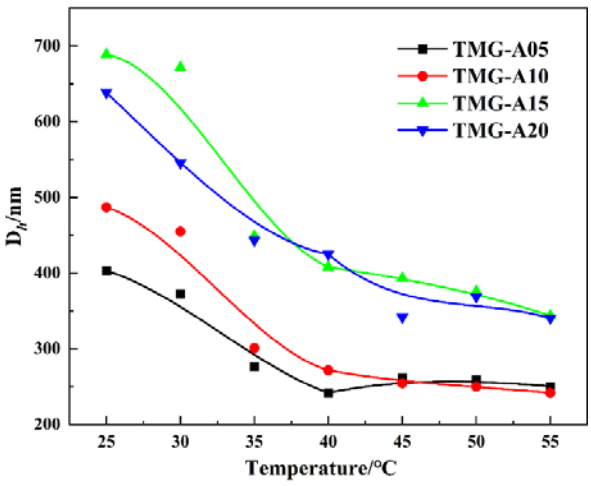

Fig. 5 D_h-temperature curves of thermo-responsive microgels with different AMPS

Fig. 5 shows the variations of Dh of poly(NIPAM-co-AMPS-co-tBA) microgel with temperature. The results show that the Dh of the microgels decreases sharply with the increase of temperature in a certain temperature range. It suggests that the microgels show good temperature sensitivity. With the increase of AMPS content in the microgel, the VPTT of the microgel increased due to the amide groups and sulfonic acid as the hydrophilic part of the microgel. The growing hydrophilic groups increased the number of hydrogen bonds between these and water molecules, leading to the VPTT of the microgel to move to a high temperature. Meanwhile, as the content of AMPS increases, the temperature sensitivity of the microgel gradually decreases.

D.Effect of tBA on Temperature-Responsive Behavior

Fig. 6 shows the Dh-temperature curves of poly(NIPAM-co-AMPS-co-tBA) microgels with different tBA contents. The

results show that the Dh of microgels decreases sharply with the increase of temperature in a certain temperature range. It implies that the microgel undergoes a bulk phase transition with increasing temperature, which proves the temperature sensitivity of poly(NIPAM-co-AMPS-co-tBA) microgel.

The VPTT of the microgels gradually decreased with the increase of hydrophobic monomer tBA ratio in the poly(NIPAM-co-AMPS-co-tBA) microgels. Meanwhile, the hydrodynamic diameter-temperature curves of the microgels demonstrates gradually flatter with the increase of hydrophobic monomers, suggesting weaker thermos-responsive behaviors. The main reason can be explained that the growing contents of the non-thermosensitive monomers, AMPS and tBA were polymerized onto the NIPAM molecular chains.

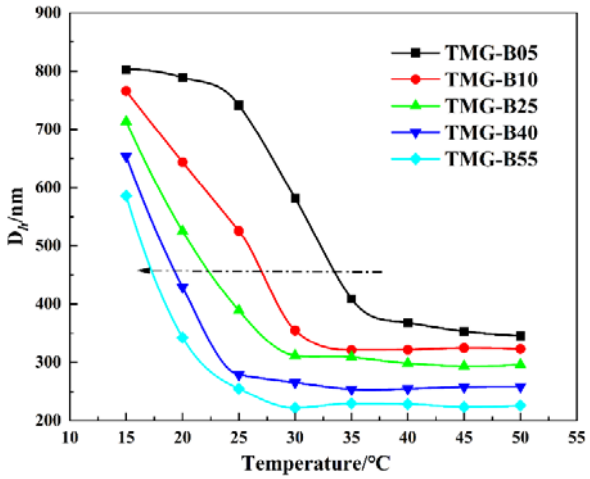

Fig. 6 D_h-temperature curves of thermo-responsive microgels with different tBA

The amide group (-CONH) and isopropyl group (-CH(CH_3)$_2$) in NIPAM, the sulfonic acid group in AMPS, and the ester group in tBA coexist in the poly(NIPAM-co-AMPS-co-tBA), resulting in the existence of a hydrophilic-hydrophobic equilibrium inside the network of the microgel. When the temperature is lower than the VPTT of the microgel, the hydrogen bonding between hydrophilic groups and water molecules in the microgel dominates the molecular chains migration, causing water molecules to gather around the microgel, which makes the microgel more hydrophilic and swollen. However, the hydrogen bonds are broken with the increase of temperature, and the molecular interactions gradually dominate by the hydrophobic interaction of the N-isopropyl groups, while the hydrophobic units on the polymer chains agglomerate with each other. Therefore, hydrophobic interaction enhanced gradually and the polymer chains displayed curl and shrink, resulting in the decrease of microgel volume and particle size.

E. Morphological Analysis

The microscopic morphologies of the microgel samples were determined by SEM and TEM. Fig. 7 shows the pictures of SEM and TEM of the microgel TMG-A15, respectively, and the embedded photos in the top right corner are the enlarged pictures. It can be found that the microgels exhibit a regular spherical shape, and the particle size distribution is homogeneous with around 200 nm. Note that the particle size obtained from Fig. 7 is slightly smaller than the particle size measured by the nano particle size analyzer at 25 °C. The reason is that microgel particles shown in TEM were obtained by drying the swollen microgel emulsion at room temperature, resulting in the degeneration of microgel structure and particle size.

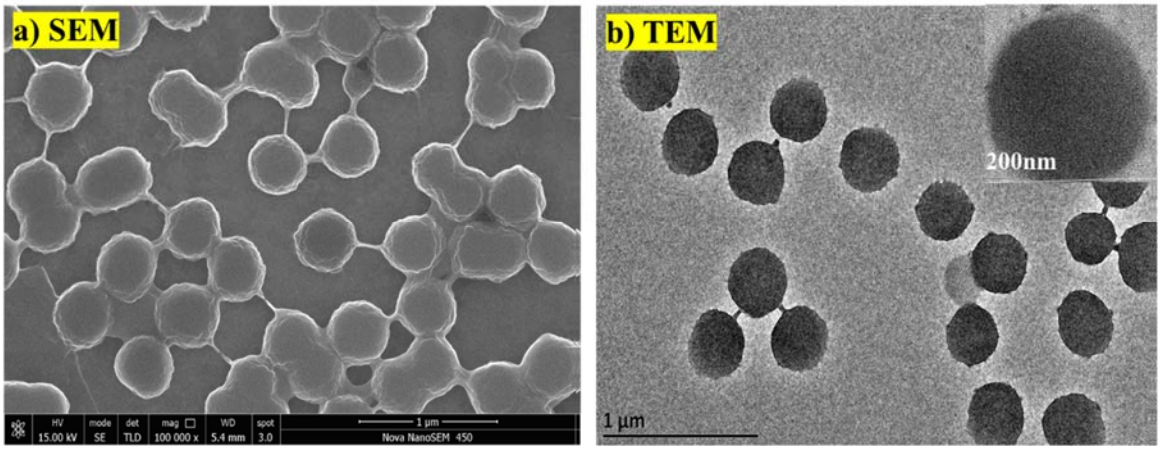

Fig. 7 SEM and TEM images of nano/microgels of the microgel TMG-A15

Fig. 8 shows the microscopic morphology of the microgels with different crosslinker contents (TMG-M03, TMG-M15). It can be seen that the prepared microgels of TMG-M03 displayed a spherical morphology and advanced polydispersity, and the particle size of the microgel particles displayed homogeneous. However, it was also found that some crosslinked aggregations are formed between particles in TMG-M15, suggesting that the excessive amount of cross-linking agent relative to the amount of NIPAM causes more nanoparticles to cluster together through the inter-particle crosslinked structures. It also leads to an increase in coagulant content and unstable emulsions.

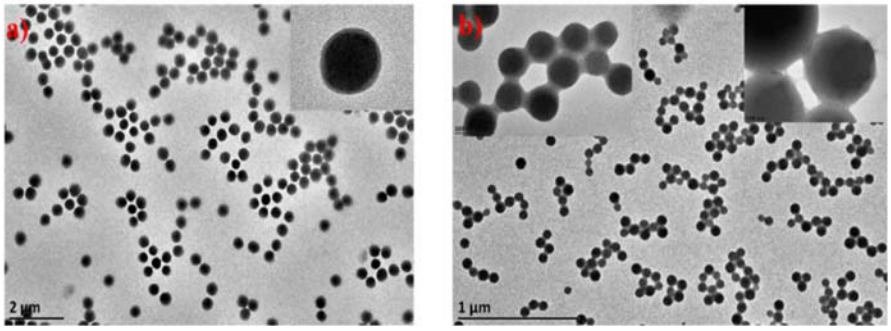

Fig. 8 TEM images of the microgels with different crosslinker contents (a)TMG-M03, (b) TMG-M15

F. Plugging Performance

To evaluate the plugging performance of the temperature-sensitive microgels in heterogeneous sediments, a core sample with a wide particle size distribution was adopted. We quantitatively measured the particle size distribution of the core using high pressure mercury intrusion tests (HPMI) which were performed by PoreMaster 33 porosimeter (Quantachrome Instruments of Anton Paar, The United States). The corresponding pore radius were calculated based on the Washburn method [29].

$$P_c = \frac{2\sigma\cos\theta}{r} \tag{1}$$

where P_c is the capillary pressure (Pa), σ is the surface tension (N/m), θ is the contact angle (degree) and r is the equivalent pore radius of core samples at the P_c. Here, the interfacial tension is 485 mN/m, and the contact angle of mercury is 140°.

According to the HPMI measurement, the PSDs cover a wide range from nanopores to micropores, indicating that various sizes of pores controlled the storage capability of tight reservoirs.

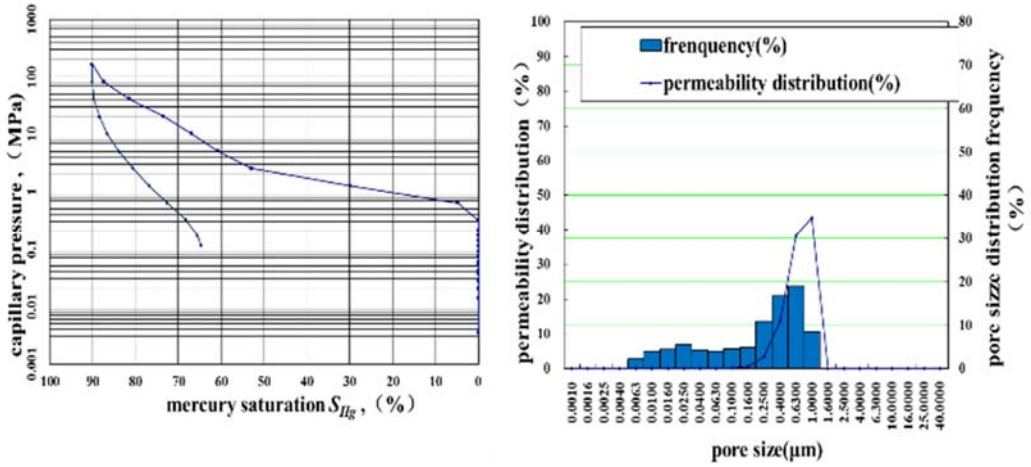

Fig. 9 Capillary curve and pore size distribution of the core sample

The core sample with heterogeneity was employed to conduct the core flow tests. To elucidate the potential self-adaptive plugging behaviors of nanogels, the injections of nanogel solution and KCl brine were conducted in the whole process. In the initial stage, we firstly performed the permeability measurement via injecting the KCl brine into the core sample. The displacement differential pressure experienced a gradual rise and then remained stable with the increase of injection time, indicating that the resistance of flow is relatively lower in the core samples. At the stage 2, the nanogel suspension was injected in to the sample to simulate the invasion of drilling fluid into formation during drilling process. Results showed that the ΔP value rocketed upwards within a short time, suggesting that the nanogel particles blocked the flow channels in the porous media. Meanwhile, it should be noted that fluctuations appeared during the injection process, indicating that the flow channel experienced continuous blocked-unblocked changes. With injection time passed by, the pressure gradually leveled off at a relatively higher value, showing the formation of compacted plugging zone in the core sample. In the stage 3, the KCl brine displacement was conducted to obtain the permeability after plugging. The ΔP value increased rapidly at the beginning, followed by a few soaring and plunging fluctuation, showing that the plugging particles migrated incessantly in the pores with the fluids flow. Finally, the pressure remained gradually stable at a relatively higher level with 1.62 MPa, five times the initial value of differential pressure.

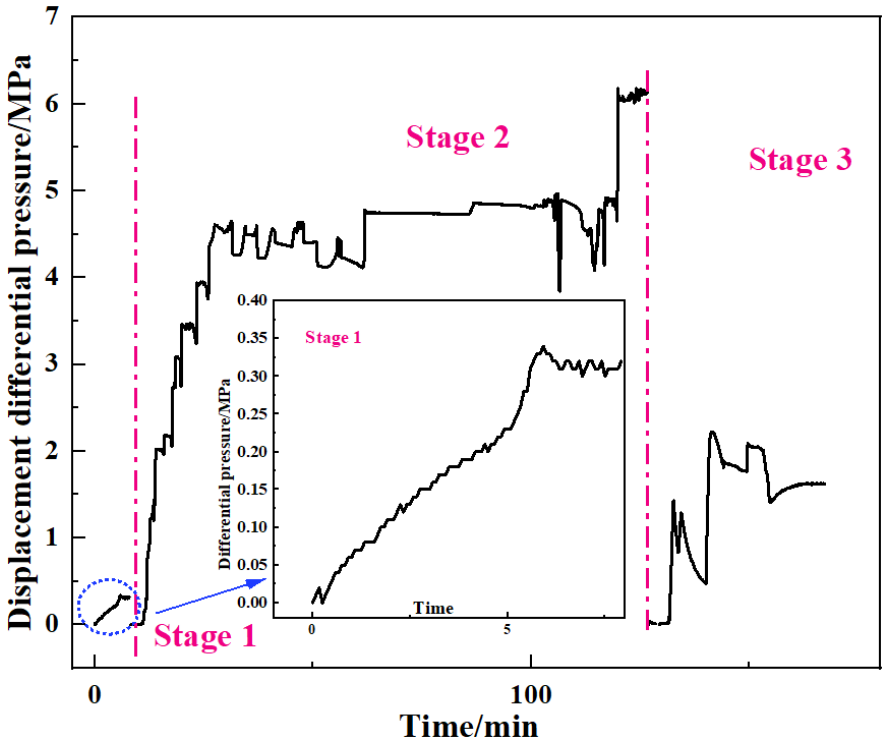

Fig. 10 The pressure curves during the plugging evaluation

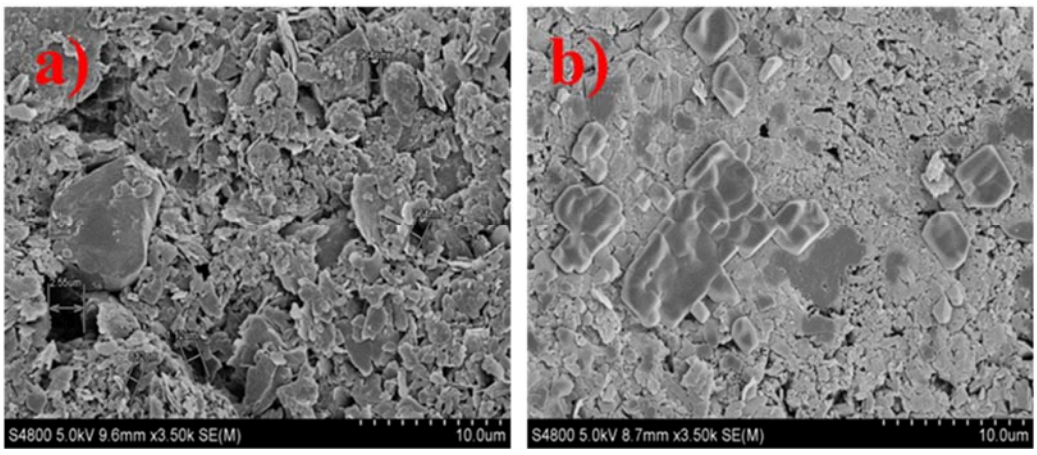

Fig. 11 SEM images of the core surfaces (a) before and (b) after displacement tests

In order to verify the microscopic mechanism of plugging in core structures, the microscopic morphology of core sample before and after core flow tests were investigated. The SEM results are shown in Fig. 11. For the initial surface of the core, a porous and rough surface was shown. However, after core flow test, obviously, we can see that the surface becomes smooth with a formed polymer film, which covered the grain and minerals, confirming that the nanogels are retained in the core structures though physical/chemical adsorption and capture. Consequently, the nanogels particles can block the flow channels, thus forming the plugging zone and degenerating the permeability.

G.Mechanism

During the drilling operations, the positive differential pressure impels nanoparticles to enter the reservoirs, randomly embedded in the pore space. The nanogels can form gradually a dense filter cake on the surface of the reservoir, effectively controlling the filtration and preventing the drilling fluid from intruding into the pore space in the sediment. However, the pore size of reservoirs varied with the well depth, and thus nanoparticles with uniform diameters might be insufficient to plug all the pore space of formation encountered during the whole drilling process. Fortunately, a series of our products with different VPTT can be employed in the drilling fluid to obtain a wide range of particle size and block the pore space for the whole drilling stage where the temperature changes with the drilling depth. As we mentioned above, when the temperature is lower than the VPTT of the microgel, the hydrogen bonding

between hydrophilic groups and water molecules in the microgel allows the microgel more hydrophilic and swollen. However, the hydrogen bonds are broken with the increase of temperature, and the molecular interactions gradually dominate by the hydrophobic interaction of the N-isopropyl groups, resulting in the decrease of microgel volume and particle size. The swelling/deswelling equilibrium provides the varied particle sizes in different temperatures.

Additionally, the microgel particles are embedded in the formation and form hydrophobic filter cakes on the surface, thereby resisting the external aqueous invasion to some extent. The hydrophobicity of pore surface can remarkably reduce the capillary force of the sediment, contributing to decrease the spontaneous imbibition volume from external drilling fluids [30]-[32]. Besides, the accumulation of polymer nanoparticles on the surface of hydrates can also inhibit the rapid decomposition of hydrates by restraining heat and mass transfer to some extent.

IV. Conclusions

In this paper, a series of thermo-responsive microgels were synthesized and characterized with different VPTT, and the plugging performance were studied in a core sample with heterogeneity.

(1) A series of temperature-sensitive microgels with different VPTTs were prepared and successfully applied as plugging agents in drilling fluids. The VPTT can be tuned by copolymerization with different molar ratios of hydrophobic monomers tBA.

(2) AMPS can reduce significantly the coagulum content in the process of copolymerization. When AMPS was added at 1.0% (relative to NIPAM), the coagulum content descended to 1.72%, and 98.62% of the monomers formed nanogel particles. An increase in the crosslinker content causes more nanoparticles to aggregate together, forming larger aggregates.

(3) AMPS can increase the VPTT of the microgel due to the growing hydrophilic groups, while the VPTT of the microgels gradually decreased with the increase of hydrophobic monomer tBA ratio. Meanwhile, as the content of AMPS or tBA increases, the temperature sensitivity of the microgel gradually decreases.

(4) A combination of nanogels with varied VPTT displays a wide particle size distribution (around 200~800 nm) near the temperature in hydrate-bearing sediments, and thus when the temperature-sensitive microgels suspension was injected into the core, the microgels provide the self-adaptive plugging capacity for the hydrate sediments to prevent external fluids from penetrating into the HBS.

References

[1] Wang J, Sun J, Wang R, Lv K, Wang J, Liao B, et al. Mechanisms of synergistic inhibition of hydrophilic amino acids with kinetic inhibitors on hydrate formation. Fuel 2022;321:124012. https://doi.org/10.1016/j.fuel.2022.124012.

[2] Liao Y, Wang Z, Sun X, Lou W, Liu H, Sun B. Modeling of hydrate dissociation surface area in porous media considering arrangements of sand grains and morphologies of hydrates. Chem Eng J 2021:133830. https://doi.org/10.1016/j.cej.2021.133830.

[3] Zhang Y, Qiu Z, Zhong H, Mu J, Ma Y, Zhao X, et al. Preparation and characterization of expanded graphite/modified n-alkanes composite phase change material for drilling in hydrate reservoir. Chem Eng J 2022;429:132422. https://doi.org/10.1016/j.cej.2021.132422.

[4] Wei J, Fang Y, Lu H, Lu H, Lu J, Liang J, et al. Distribution and characteristics of natural gas hydrates in the Shenhu Sea Area, South China Sea. Mar Pet Geol 2018;98:622–8. https://doi.org/10.1016/j.marpetgeo.2018.07.028.

[5] Zhang Y, Qiu Z, Zhong H, Mu J, Ma Y, Zhao X, et al. Preparation and characterization of expanded graphite/modified n-alkanes composite phase change material for drilling in hydrate reservoir. Chem Eng J 2022;429:132422. https://doi.org/10.1016/j.cej.2021.132422.

[6] Sun W, Pei J, Wei N, Zhao J, Xue J, Zhou S, et al. Sensitivity analysis of reservoir risk in marine gas hydrate drilling. Petroleum 2021;7:427–38. https://doi.org/10.1016/j.petlm.2021.10.013.

[7] Fereidounpour A, Vatani A. An investigation of interaction of drilling fluids with gas hydrates in drilling hydrate bearing sediments. J Nat Gas Sci Eng 2014;20:422–7. https://doi.org/10.1016/j.jngse.2014.07.006.

[8] Zheng M, Liu T, Jiang G, Wei M, Huo Y, Liu L. Large-scale and high-similarity experimental study of the effect of drilling fluid penetration on physical properties of gas hydrate-bearing sediments in the Gulf of Mexico. J Pet Sci Eng 2020;187:106832. https://doi.org/10.1016/j.petrol.2019.106832.

[9] Kuang Y, Yang L, Li Q, Lv X, Li Y, Yu B, et al. Physical characteristic analysis of unconsolidated sediments containing gas hydrate recovered from the Shenhu Area of the South China sea. J Pet Sci Eng 2019;181:106173. https://doi.org/10.1016/j.petrol.2019.06.037.

[10] Zhong H, Gao X, Qiu Z, Sun B, Huang W, Li J. Insight into β-cyclodextrin polymer microsphere as a potential filtration reducer in water-based drilling fluids for high temperature application. Carbohydr Polym 2020;249:116833. https://doi.org/10.1016/j.carbpol.2020.116833.

[11] Lei M, Huang W, Sun J, Shao Z, Chen Z, Chen W. Synthesis and characterization of high-temperature self-crosslinking polymer latexes and their application in water-based drilling fluid. Powder Technol 2021;389:392–405. https://doi.org/10.1016/j.powtec.2021.05.045.

[12] Lei M, Huang W, Sun J, Shao Z, Zhao L, Zheng K, et al. Synthesis and characterization of thermo-responsive polymer based on carboxymethyl chitosan and its potential application in water-based drilling fluid. Colloids Surf Physicochem Eng Asp 2021;629:127478. https://doi.org/10.1016/j.colsurfa.2021.127478.

[13] Liu F, Yao H, Liu Q, Wang X, Dai X, Zhou M, et al. Nano-silica/polymer composite as filtrate reducer in water-based drilling fluids. Colloids Surf Physicochem Eng Asp 2021;627:127168. https://doi.org/10.1016/j.colsurfa.2021.127168.

[14] Qin X, Liang Q, Ye J, Yang L, Qiu H, Xie W, et al. The response of temperature and pressure of hydrate reservoirs in the first gas hydrate production test in South China Sea. Appl Energy 2020;278:115649. https://doi.org/10.1016/j.apenergy.2020.115649.

[15] Wei J, Liang J, Lu J, Zhang W, He Y. Characteristics and dynamics of gas hydrate systems in the northwestern South China Sea - Results of the fifth gas hydrate drilling expedition. Mar Pet Geol 2019;110:287–98. https://doi.org/10.1016/j.marpetgeo.2019.07.028.

[16] Ye J, Wei J, Liang J, Lu J, Lu H, Zhang W. Complex gas hydrate system in a gas chimney, South China Sea. Mar Pet Geol 2019;104:29–39. https://doi.org/10.1016/j.marpetgeo.2019.03.023.

[17] Atta AM. Surface-active amphiphilic poly[(2-acrylamido-2-methylpropanesulfonic acid)-co-(N-isopropylacrylamide)] nanoparticles as stabilizer in aqueous emulsion polymerization. Polym Int 2014;63:607–15. https://doi.org/10.1002/pi.4537.

[18] Jones CD, Lyon LA. Synthesis and Characterization of Multiresponsive Core−Shell Microgels. Macromolecules 2000;33:8301–6. https://doi.org/10.1021/ma001398m.

[19] Berndt I, Pedersen JS, Richtering W. Temperature-Sensitive Core–Shell Microgel Particles with Dense Shell. Angew Chem 2006;118:1769–73. https://doi.org/10.1002/ange.200503888.

[20] Hamzah YB, Hashim S, Rahman WAWA. Synthesis of polymeric nano/microgels: a review. J Polym Res 2017;24:134. https://doi.org/10.1007/s10965-017-1281-9.

[21] Serrano-Medina A, Cornejo-Bravo JM, Licea-Claveríe A. Synthesis of pH and temperature sensitive, core–shell nano/microgels, by one pot, soap-free emulsion polymerization. J Colloid Interface Sci 2012;369:82–90. https://doi.org/10.1016/j.jcis.2011.12.045.

[22] Kubo M, Higuchi M, Koshimura T, Shoji E, Tsukada T. Control of the temperature responsiveness of poly(N-isopropylacrylamide-co-2-

hydroxyethyl methacrylate) copolymer using ultrasonic irradiation. Ultrason Sonochem 2021;79:105752. https://doi.org/10.1016/j.ultsonch.2021.105752.
[23] Wang J, Chen Y, An J, Xu K, Chen T, Müller-Buschbaum P, et al. Intelligent Textiles with Comfort Regulation and Inhibition of Bacterial Adhesion Realized by Cross-Linking Poly(n-isopropylacrylamide-co-ethylene glycol methacrylate) to Cotton Fabrics. ACS Appl Mater Interfaces 2017;9:13647–56. https://doi.org/10.1021/acsami.7b01922.
[24] Huang Z-S, Shiu J-W, Way T-F, Rwei S-P. A thermo-responsive random copolymer of poly(NIPAm-co-FMA) for smart textile applications. Polymer 2019;184:121917. https://doi.org/10.1016/j.polymer.2019.121917.
[25] Feng M, Kong X, Feng Y, Li X, Luo N, Zhang L, et al. A New Reversible Thermosensitive Liquid–Solid TENG Based on a P(NIPAM-MMA) Copolymer for Triboelectricity Regulation and Temperature Monitoring. Small n.d.;n/a:2201442. https://doi.org/10.1002/smll.202201442.
[26] Ji Y, Hou J, Cui G, Lu N, Zhao E, Liu Y, et al. Experimental study on methane hydrate formation in a partially saturated sandstone using low-field NMR technique. Fuel 2019;251:82–90. https://doi.org/10.1016/j.fuel.2019.04.021.
[27] Chong ZR, Yang M, Khoo BC, Linga P. Size Effect of Porous Media on Methane Hydrate Formation and Dissociation in an Excess Gas Environment. Ind Eng Chem Res 2016;55:7981–91. https://doi.org/10.1021/acs.iecr.5b03908.
[28] Zhan L, Wang Y, Li X-S. Experimental study on characteristics of methane hydrate formation and dissociation in porous medium with different particle sizes using depressurization. Fuel 2018;230:37–44. https://doi.org/10.1016/j.fuel.2018.05.008.
[29] Kumar A, Maini B, P.R. Bishnoi, Clarke M, Zatsepina O, Srinivasan S. Experimental determination of permeability in the presence of hydrates and its effect on the dissociation characteristics of gas hydrates in porous media. J Pet Sci Eng 2010;70:114–22. https://doi.org/10.1016/j.petrol.2009.10.005.
[30] Zhang L, Dong H, Dai S, Kuang Y, Yang L, Wang J, et al. Effects of depressurization on gas production and water performance from excess-gas and excess-water methane hydrate accumulations. Chem Eng J 2022;431:133223. https://doi.org/10.1016/j.cej.2021.133223.
[31] Liu Z, Chen L, Wang Z, Gao Y, Wang J, Yu C, et al. Hydrate phase equilibria in natural sediments: Inhibition mechanism and NMR-based prediction method. Chem Eng J 2023;452:139447. https://doi.org/10.1016/j.cej.2022.139447.
[32] Li B, Li X-S, Li G, Jia J-L, Feng J-C. Measurements of Water Permeability in Unconsolidated Porous Media with Methane Hydrate Formation. Energies 2013;6:3622–36. https://doi.org/10.3390/en6073622.